111 COMPARING GPM SATELLITE TO GROUND PLATFORM MEASUREMENTS: CASE STUDIES FROM THE NASA GPM WALLOPS PRECIPITATION SCIENCE RESEARCH FACILITY

Charanjit S. Pabla[1,2,*], S. M. Wingo[3], D. B. Wolff[2], D. A. Marks[1,2],
W. A. Petersen[4], A. Tokay[5,6], and P. N. Gatlin[4]

Science Systems and Applications, Inc, Lanham, MD[1]
NASA Goddard Space Flight Center – Wallops Flight Facility, Wallops Island, VA[2]
NASA Marshal Space Flight Center and Universities Space Research Association, Huntsville, AL[3]
NASA Marshal Space Flight Center, Huntsville, AL[4]
Joint Center for Earth Systems Technology, University of Maryland, Baltimore County[5]
NASA Goddard Space Flight Center, Greenbelt, MD[6]

1. INTRODUCTION

The NASA Global Precipitation Measurement (GPM) mission is crucial in understanding the global distribution (both horizontal and vertical) of precipitation to improve weather forecasting and climate modeling. GPM Core Observatory was launched into orbit February 27, 2014 with mission lifetime of about 3 years, which might extend to more than 15 years based on fuel consumption and instrument performance (Skofronick-Jackson et al. 2017). For the success of GPM, a careful Ground Validation (GV) must be performed using a spectrum of ground instruments (e.g., dense rain gauges, ground scanning and profiling radars, disdrometers) with keeping in mind that ground measurements—which have their own errors and uncertainties—also do not represent the exact truth (Hou et al. 2014). GPM GV is crucial because it provides critical feedback to algorithm developers on biases between ground measurements and satellite retrievals. Knowledge of the horizontal and vertical distribution of precipitation within an atmospheric column is important to bridge the gap between space- and ground-based measurements.

This study focuses on analyzing GPM Core Observatory overpass events at NASA Wallops Precipitation Research Facility (PRF), where a spectrum of research quality precipitation instruments are deployed for operations on a daily basis.

2. DATA AND OBSERVATIONS

Data considered in this research come from an array of instruments: NASA's S-band Dual-Polarimetric Radar (NPOL), Ka/Ku-band Dual-Polarization Dual-frequency Doppler Radar (D3R), K-band Micro Rain Radar (MRR), National Weather Service (NWS) dual-polarimetric S-band Weather Surveillance Radars 1988 Doppler (WSR-88D), GPM multi-channel Microwave Imager (GMI) and Ka/Ku-band Dual-frequency Precipitation Radar (DPR), 2-Dimensional Video Disdrometer (2DVD), Particle Size and Velocity (PARSIVEL) disdrometer, and dual tipping rain gauges.

Two GPM short distance (< 60 km from nadir track and NPOL site) overpass events over the Wallops Flight Facility are considered for this study. The first overpass event occurred on 21 May 2015 (Figure 1a) and the second on 28 June 2016 (Figure 1b). These two events were chosen among many others due to excellent GPM GMI, Ku, and Ka swath coverage below precipitating storms and ground observations.

3. ANALYSIS SET-UP

The System for Integrating Multi-platform data to Build the Atmospheric column or SIMBA (Wingo et al. 2017) framework is exploited to feed in data from an array of platforms and produce an atmospheric column product. The idea of this approach is to combine data from various platforms into a common gridded column to infer GPM sensor bias and uncertainties related to different precipitation environments (e.g., light stratiform vs. convective). Additionally, this framework allows studying the vertical profile of drop size distribution and precipitation variability from different instruments in a common location.

In order to conduct this research, a grid center location and extent was chosen on the eastern shore of Virginia over NASA's Wallops Island PRF. The grid has a vertical and horizontal extent of 5 x 5 x 5 km and a grid spacing of 500 m in all directions to be consistent with GPM DPR nadir footprint (Iguchi et al. 2016). The grid center is directly over a test pad (WFF Pad) containing rain gauges, disdrometers, and MRR instruments, and within coverage of the D3R. With the column grid specified and the ground and satellite data as inputs, SIMBA generates a netCDF file with the concomitant fields from each available sensor set into the 3D column grid. The final step includes computing statistics (average and bias error). The average is computed in the horizontal direction (5 x 5 km) at each height level up to 5.0 km. The bias is computed as follows

* *Corresponding author address:* Charanjit S. Pabla, GPM-GV, NASA Goddard Space Flight Center – Wallops Flight Facility, Code 610.W, Wallops Island, VA 23337; email: charanjit.s.pabla@nasa.gov

$$bias = \frac{Satellite - GV}{GV},$$

where *Satellite* refers to GPM (either GMI or DPR products) and *GV* refers to ground scanning/profiling radar, disdrometer, or rain gauge measurements.

3.1 Algorithms

As part of one of the Level 1 mission requirements, DPR is to accurately retrieve the drop size distribution parameters from which rain rates are retrieved using simultaneous measurements from Ku- and Ka-PR frequencies (Seto et al. 2013). Rainfall rate highly depends on the raindrop size distribution. GPM DPR algorithms adopt the 3-parameter normalized gamma distribution, namely mass-weighted mean diameter (D_m, mm), normalized intercept parameter (N_w, mm^{-1} m^{-3}) and shape parameter (μ). The GPM DPR Level-2 (2ADPR) Version 5 algorithm developed by the DPR Algorithm Development Team provides reflectivity, precipitation rate, and the drop size distribution measurements used in this study (Kubota et al. 2014; Iguchi et al. 2016). DPR algorithms can be broken down into three scan types: normal scan (NS), matched scan (MS), and high sensitivity scan (HS) which relate to multiple operational modes of Ka Precipitation Radar (KaPR) and single operational mode from KuPR with a horizontal resolution of 5.0 km as described in Iguchi et al. (2012), Kubota et al. (2014) and Iguchi et al. (2016).

3.2 D_m and N_w

D_m is the ratio of the fourth and third moments of the drop size distribution, N_w is proportional to the liquid water content, and μ is the shape parameter of the gamma distribution (set to 3.0 in GPM algorithms). The drop-size distribution parameters (N_w and D_m) for GV radars are estimated using dual-polarization variables following Gorgucci et al. (2002) and Bringi et al. (2004) methods according to NASA's GPM-GV DSD retrievals flowchart (Tokay et al. 2017). On the other hand, the GPM 2ADPR retrievals rely on the Ka and Ku dual-frequency reflectivity measurements to derive N_w and D_m (Seto et al. 2013).

3.3 Rain Rate

Rain rate retrieved from GV radars (NPOL, KDOX, KAKQ) utilizes the DROPS2.0 algorithm (Chen et al. 2017). This algorithm is an improvement to the Colorado State University (CSU) hydrometeor identification (HID) or CSU-HIDRO (Cifelli et al. 2011) which takes advantage of the polarimetric variables along with regional hydrometeor classification technique to estimate rain rate.

GPM 2ADPR takes advantage of a revised R-D_m relation, first adopted in GPM DPR algorithms (Version 04 and 05) after using the k-Ze and Z-R relation in previous algorithm (Version 03) to estimate rain rate (Kazo et al. 2009; Seto et al. 2016). D_m is estimated directly in GPM-DPR algorithms as discussed previously.

GPM GMI uses the Goddard profiling (GPROF) algorithm which is a Bayesian technique that involves the brightness temperature of clouds and precipitation particles calculated from radiative transfer equations and cloud resolving model output to estimate rainfall rate (Kummerow et al. 1996, 2015).

Surface instruments (2DVD and APU) provide rain rates using direct DSD measurements (refer to Tokay et al. 2001 for more details) while gauge rainfall rates are estimated using techniques discussed in Wang et al. (2008).

4. RESULTS AND INTERPRETATION

4.1 GPM OP 21 May 2015

A widespread stratiform rainfall event occurred over the Delmarva region under a short distance from nadir and NPOL (45.8 km) GPM Core Observatory overpass. NASA's NPOL radar captured this event (see Figure 2) along with a majority of the WFF Pad ground-based instruments. The stratiform rain case provided a good starting point for an analysis based on the atmospheric column product generated by the SIMBA data fusion framework. Note the timestamps of input data in SIMBA ranged from +/-180 seconds of NPOL scan time. SIMBA data inventory for this event is listed in the left column of Table 1.

The mean over the whole 5 x 5 km at each column grid vertical level corrected reflectivity profile (Figure 3) shows how well each platform or algorithm compares against GPM DPR. Important to note that GV radars (NPOL, KDOX, KAKQ) reflectivity has not been adjusted for the higher DPR and D3R frequencies in the comparisons. The mean vertical profile of reflectivity from DPR (2ADPR algorithm) is generally higher compared to NPOL, KDOX, KAKQ, and D3R. Further, notice the clustering of surface observations from APU and 2ADPR mean reflectivity near 30 dBZ. In this case, 2DVD is the outlier with a mean reflectivity of 34 dBZ. Generally, the vertical profiles look decent with some variability in the SIMBA column.

The mean over the whole 5 x 5 km at each column grid vertical level rainfall rate (mm hr^{-1}) profiles are shown in Figure 4 for this case. Notice KDOX and KAKQ average vertical profiles are nearly constant with height at around 0.5 mm hr^{-1} while 2ADPR and NPOL show decreasing signatures from near the surface around 2.0 mm hr^{-1} up to the freezing level near 0.0 mm hr^{-1}. Within the column, 2ADPR algorithm has an increasingly negative trend in bias with height relative to GV radars. Moreover, average rain rate variability from near surface ranged from 1.0

mm hr^{-1} to as high as 7.0 mm hr^{-1}. GMI-GPROF algorithm underestimated rain rate relative to all ground measurements (MRR, APU, Gauges, and 2DVD) with an average bias of -80% (see Table 2). The 2ADPR surface rain rate algorithm generally underestimated rain rate relative to all ground platforms except Gauges. The 2ADPR rain rate bias ranged from -40 to -70% while nearly zero biased relative to Gauges. Overall, the stratiform rain event vertical profile of rain rate among different platforms and algorithms differ quite a bit possibly due to DSD variability and/or uncertainties in algorithm assumptions.

Since DSD is crucial for accurately retrieving rainfall rate, it is important to analyze vertical profile of the DSD parameters. The mean over the whole 5 x 5 km at each column grid vertical level mass-weighted mean diameter, D_m shown in Figure 5 has values between 1.0 mm near the surface to about 1.6 mm in the column, below the freezing level. Further, 2ADPR algorithm has an increasingly negative trend in bias with height relative to NPOL, KDOX, and KAKQ ground radars. The bias ranges between -50 to about +50% throughout the column depending on which 2ADPR algorithm (i.e., HS, NS, or MS) is considered.

The mean over the whole 5 x 5 km at each column grid vertical level normalized intercept parameter, log N_w shown in Figure 6 has values between 3.0 and 5.0 in the column, below the freezing level. Additionally, 2ADPR algorithm has an increasingly positive trend in bias with height relative to GV radars. The bias is between -30 and +30% throughout the column.

Plotting the mean N_w and D_m on the same plot for each instrument as a function of height shows an interesting inverse relationship between the two DSD parameters (Figure 7). The inverse relationship (ignoring the height dependence) along with mean D_m and N_w values fall within the range found in literature (Bringi et al. 2003; Chandrasekar et al. 2008). They found clusters of average D_m between 1.25 and 1.75 mm and log N_w between 3.0 and 4.0 in stratiform rain from different climatic regions around the world from disdrometer and polarimetric radar measurements. Thus, the mean DSD parameters in the stratiform vertical profile in our analysis are consistent with past studies.

4.2 GPM OP 28 June 2016

Contrary to the previous event, NPOL captured a mixed stratiform and convective rain event under a short distance from nadir and NPOL (53.6 km) GPM Core Observatory overpass (Figure 8). Note the SIMBA column grid was moved 4.2 km north of WFF Pad for this case due to reflectivity gradients (see close-up view of NPOL in Figure 8) in NPOL data. Due to this adjustment, there was no data from the ground instruments (2DVD, APU, Gauges, MRR) for this case. Timestamps of input data in SIMBA ranged from +/-200 seconds of NPOL scan time. SIMBA data inventory for this event is listed on the right in Table 1.

Figure 9 shows the mean over the whole 5 x 5 km at each column grid vertical level corrected reflectivity profiles from this event. Similar to last event, there is no adjustment made to NPOL, KDOX, and KAKQ reflectivity to higher frequencies of DPR and D3R for comparison. Interestingly, the mean vertical profile of reflectivity from 2ADPR algorithm is sandwiched between the ground scanning radars generally, with NPOL having the highest values of reflectivity while D3R has the lowest values within the column and below the freezing level (i.e., D3R < KAKQ < DPR < KDOX < NPOL). Furthermore, the 2ADPR near surface algorithm shows mean reflectivity between 35 to 38 dBZ. Note the enhanced dBZ values for D3R and NPOL just below the freezing level at 4.0 km. Due to the higher sensitivity of D3R and NPOL measurements (both corrected for attenuation and not adjusted for frequency differences), the melting signature or bright band is evident in the reflectivity profile just below 4.0 km compared to DPR and the WSR-88Ds. There is some decent variability of reflectivity within the SIMBA grid column for this convective/stratiform case.

The mean over the whole 5 x 5 km at each column grid vertical level profile of rainfall rate (mm hr^{-1}) for this convective case is shown in Figure 10. There is considerable variability in rain rate throughout the column. For example, KDOX and NPOL exhibit the largest average rates from about 10.0 to 15.0 mm hr^{-1} near the surface to 15.0 to 20.0 mm hr^{-1} just below the freezing level compared to KAKQ and 2ADPR ranging from about 5.0 to 8.0 mm hr^{-1} near the surface to about 5.0 mm hr^{-1} just below the freezing level. The 2ADPR bias relative to ground radars is between -80 and 0% within the SIMBA grid column, which indicates DPR underestimates relative to GV radars. Overall, decent variability is identified in the SIMBA grid column among different instruments for this convective case.

The DSD parameter D_m shown in Figure 11 has mean over the whole 5 x 5 km at each column grid vertical level values between 1.3 and 2.2 mm within the column. Similar to NPOL reflectivity enhancement near 4.0 km, NPOL mean D_m exhibits a maximum of 2.2 mm while the other instruments miss this important signature, especially DPR. The 2ADPR algorithm is slightly positively biased relative to 88Ds, which are further away from the SIMBA grid than NPOL. The bias is in the range of -20 to +20% throughout the column.

The mean over the whole 5 x 5 km at each column grid vertical level Log N_w shown in Figure 12 has values between 3.5 and 5.0 within the column. Note that just just below 4.0 km, mean Log N_w derived from NPOL experiences a minimum, collocated with the maximum mean reflectivity and mean D_m, signifying a transition zone (bright band signature). None of the

other algorithms picked up on this important signature, especially 2ADPR algorithm in consideration. The 2ADPR algorithm has a bias in the range of -30 to -20% in the column.

Similar to the previous case, a plot of mean N_w vs mean D_m is shown in Figure 13 for this event. The average values of each DSD parameter do match the range given in Bringi et al. (2003) and Chandrasekar et al. (2008). In summary, our results are consistent with past literature.

5 SUMMARY

GPM GV is very important for the scientific community to validate space-based precipitation and DSD algorithms to enhance precipitation forecasting in numerical weather prediction and flood prediction. In order to bridge the gap between space and ground based instrument measurements within a common atmospheric column, the SIMBA (Wingo et al. 2017) data fusion tool was exploited in this study. Two different GPM Core Observatory overpass events were analyzed over the Wallops Precipitation Research Facility on Wallops Island, VA. Specifically, radar reflectivity measurements and bias error of instantaneous precipitation rate and raindrop size distribution parameters obtained from ground observations and GPM GMI and DPR were compared within an atmospheric column.

The mean over the whole 5 x 5 km at each column grid vertical level reflectivity profile from 2ADPR was generally higher compared to ground-based scanning radars in a stratiform rain environment while sandwiched between the ground-based radars in the convective case. Interestingly, 2ADPR rain rate had an increasingly negative trend in bias with height relative to ground-based radars in both the stratiform and convective rain events. GMI-GPROF and 2ADPR near surface algorithms underestimated rain rate compared to all ground-based measurements in the stratiform rain event. The ground-based measurements were not available for the convective event due to shifting of the SIMBA grid location as a consequence of gradients in NPOL data. In terms of the rain DSD parameters, 2ADPR D_m algorithm had an increasingly negative trend in bias with height relative to ground-based radars while 2ADPR log N_w algorithm had an increasingly positive trend in bias in the stratiform rain case. In the convective case, the DSD parameters did not exhibit any bias trends within the SIMBA column grid. Importantly, 2ADPR algorithm missed the bright band signature in the convective case compared to NPOL data possibly due to the nature of the meteorology and courser resolution compared to NPOL.

The cause of the biases can be a number of reasons: differing distance/height of GV radars, data vertical resolution (KDOX, KAKQ PPI vs. NPOL RHI), beam filling errors, gridding/interpolation artifacts, and finally microphysical assumptions in the algorithms. A robust agreement between GPM and GV is difficult to obtain on a case by case basis thus a thorough case analysis and the inclusion of a large number of case studies is required to draw concrete conclusions on possible uncertainties.

6. ACKNOWLEDGMENTS

This research is funded by Dr. Ramesh Kakar, NASA PMM and Dr. Gail Skofronick-Jackson, NASA GPM Project Scientist. We would also like to thank Jason Pippitt for NPOL radar data processing, Jianxin Wang for gauge data processing, Dr. V. Chandrasekar's group at CSU for D3R data processing, Mike Watson and Gary King for NPOL maintenance, and Jason Bashor and rest of the ground instrument team at WFF for gauge and disdrometer maintenance.

7. REFRERENCES

Bringi, V. N., V. Chandrasekar, J. Hubbert, E. Gorgucci, W. L. Randeu, and M. Schoenhuber, 2003: Raindrop size distribution in different climatic regimes from disdrometer and dual-polarized radar analysis. *Journal of the Atmospheric Sciences*, **60 (2)**, 354–365, doi:10.1175/ 1520-0469(2003)060⟨0354:RSDIDC⟩2.0.CO;2.

Bringi, V. N., T. Tang, and V. Chandrasekar, 2004: Evaluation of a new polarimetrically based zr relation. *Journal of Atmospheric and Oceanic Technology*, **21 (4)**, 612–623, doi:10.1175/ 1520-0426(2004)021⟨0612:EOANPB⟩2.0.CO;2.

Chandrasekar, V., V. Bringi, S. Rutledge, A. Hou, E. Smith, G. S. Jack- son, E. Gorgucci, and W. Petersen, 2008: Potential role of dual-polarization radar in the validation of satellite precipitation measurements: Rationale and opportunities. *Bulletin of the American Meteorological Society*, **89 (8)**, 1127–1145.

Chen, H., V. Chandrasekar, and R. Bechini, 2017: An improved dual-polarization radar rainfall algorithm (drops2.0): Application in nasa ifloods field campaign. *Journal of Hydrometeorology*, **18 (4)**, 917– 937, doi:10.1175/JHM-D-16-0124.1.

Cifelli, R., V. Chandrasekar, S. Lim, P. C. Kennedy, Y. Wang, and S. A. Rutledge, 2011: A new dual-polarization radar rainfall algorithm: Application in

colorado precipitation events. *Journal of Atmospheric and Oceanic Technology*, **28 (3)**, 352–364, doi:10.1175/ 2010JTECHA1488.1.

Gorgucci, E., V. Chandrasekar, V. Bringi, and G. Scarchilli, 2002: Estimation of raindrop size distribution parameters from polarimetric radar measurements. *Journal of the Atmospheric Sciences*, **59 (15)**, 2373–2384.

Hou, A. Y., and Coauthors, 2014: The global precipitation measurement mission. *Bulletin of the American Meteorological Society*, **95 (5)**, 701–722.

Iguchi, T., S. Seto, R. Meneghini, N. Yoshida, J. Awaka, M. Le, V. Chandrasekar, and T. Kubota, 2017: *GPM/DPR Level-2 Algorithm Theoretical Basis Document*. URL https://pps.gsfc.nasa.gov/Documents/ATBD DPR 201708 whole 1.pdf.

Iguchi, T., and Coauthors, 2012: An overview of the precipitation retrieval algorithm for the dual-frequency precipitation radar (dpr) on the global precipitation measurement (gpm) missions core satellite. *Proc. SPIE Earth Observ. Missions Sens.: Dev. Implement. Charact. II*, Vol. 8528, 85281C.

Kozu, T., T. Iguchi, T. Kubota, N. Yoshida, S. Seto, J. Kwiatkowski, and Y. N. Takayabu, 2009: Feasibility of raindrop size distribution parameter estimation with trmm precipitation radar. *Journal of the Meteorological Society of Japan*, **87A**, 53–66, doi:10.2151/jmsj.87A. 53.

Kubota, T., and Coauthors, 2014: Evaluation of precipitation estimates by at-launch codes of gpm/dpr algorithms using synthetic data from trmm/pr observations. *IEEE Journal of Selected Topics in Applied Earth Observations and Remote Sensing*, **7 (9)**, 3931–3944, doi:10.1109/JSTARS.2014.2320960.

Kummerow, C., W. S. Olson, and L. Giglio, 1996: A simplified scheme for obtaining precipitation and vertical hydrometeor profiles from passive microwave sensors. *IEEE Transactions on Geoscience and Remote Sensing*, **34 (5)**, 1213–1232.

Kummerow, C. D., D. L. Randel, M. Kulie, N.-Y. Wang, R. Ferraro, S. J. Munchak, and V. Petkovic, 2015: The evolution of the goddard profiling algorithm to a fully parametric scheme. *Journal of Atmospheric and Oceanic Technology*, **32 (12)**, 2265–2280, doi: 10.1175/JTECH- D- 15- 0039.1.

Seto, S., T. Iguchi, and T. Oki, 2013: The basic performance of a precipitation retrieval algorithm for the global precipitation measurement mission's single/dual-frequency radar measurements. *Geoscience and Remote Sensing, IEEE Transactions on*, **51 (12)**, 5239– 5251.

Seto, S., T. Shimozuma, T. Iguchi, and T. Kozu, 2016: Spatial and temporal variations of mass-weighted mean diameter estimated by gpm/dpr. *IEEE International*, 3938–3940.

Skofronick-Jackson, G., and Coauthors, 2017: The global precipitation measurement (gpm) mission for science and society. *Bulletin of the American Meteorological Society*, **98 (8)**, 1679–1695, doi:10.1175/ BAMS-D-15- 00306.1.

Tokay, A., L. P. D'Adderio, D. A. Marks, J. L. Pippitt, D. B. Wolff, and W. A. Petersen, 2017: Development of the raindrop size distribution parameters for the nasa global precipitation measurement mission ground validation program. *Journal of Atmospheric and Oceanic Technology*. Manuscript in preparation.

Tokay, A., L. P. DAdderio, D. B. Wolff, and W. A. Petersen, 2016: A field study of pixel-scale variability of raindrop size distribution in the mid-atlantic region. *Journal of Hydrometeorology*, **17 (6)**, 1855– 1868, doi:10.1175/JHM-D-15-0159.1.

Tokay, A., A. Kruger, and W. F. Krajewski, 2001: Comparison of drop size distribution measurements by impact and optical disdrometers. *Journal of Applied Meteorology*, **40 (11)**, 2083–2097, doi:10.1175/ 1520-0450(2001)040⟨2083:CODSDM⟩2.0.CO;2.

Wang, J., B. L. Fisher, and D. B. Wolff, 2008: Estimating rain rates from tipping-bucket rain gauge measurements. *Journal of Atmospheric and Oceanic Technology*, **25 (1)**, 43–56, doi:10.1175/

2007JTECHA895.1.

Wingo, S. M., W. A. Petersen, P. N. Gatlin, D. A. Marks, C. S. Pabla, and D. B. Wolff, 2017: Applying the simba data fusion framework to olympex: Multi-platform observational analysis of an in-tensively sampled orographically enhanced precipitation event. *38th AMS Conference on Radar Meteorology*, URL https://ams.confex.com/ams/38RADAR/meetingapp.cgi/Paper/320546.

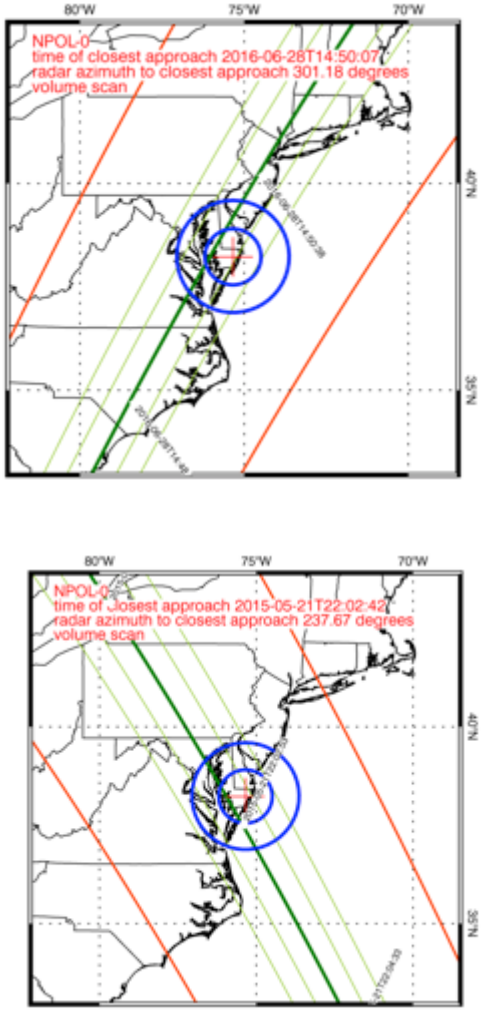

Figure 1: GPM short distance from nadir and NPOL site (< 60 km) overpass over the Delmarva on a) 21 May 2015 and b) 28 June 2016.

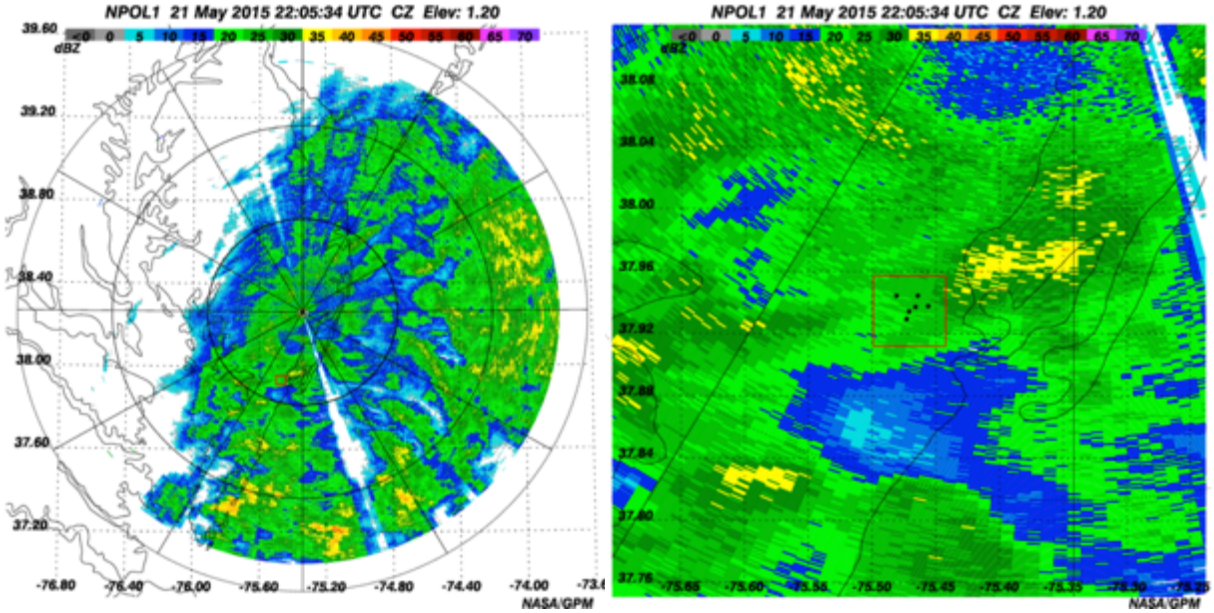

Figure 2: NPOL PPI attenuation corrected reflectivity on 21 May 2015 at 220534 UTC at 1.2° elevation a) full view and b) close up over the SIMBA column grid (boxed) with black symbols representing locations of 2DVDs. Range rings are 50 km intervals.

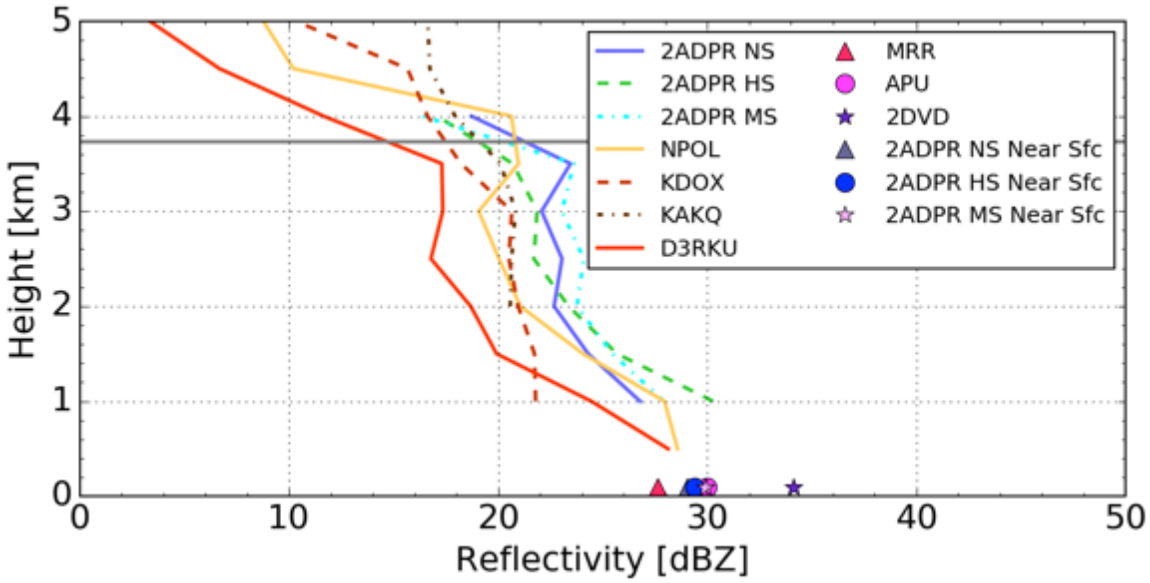

Figure 3: Mean attenuation corrected reflectivity profile from a number of platforms and algorithms. S-band reflectivity data (e.g., NPOL, KDOX, KAKQ) is not adjusted to Ku or Ka frequency for comparison. The horizontal solid line near 4.0 km indicates the freezing level.

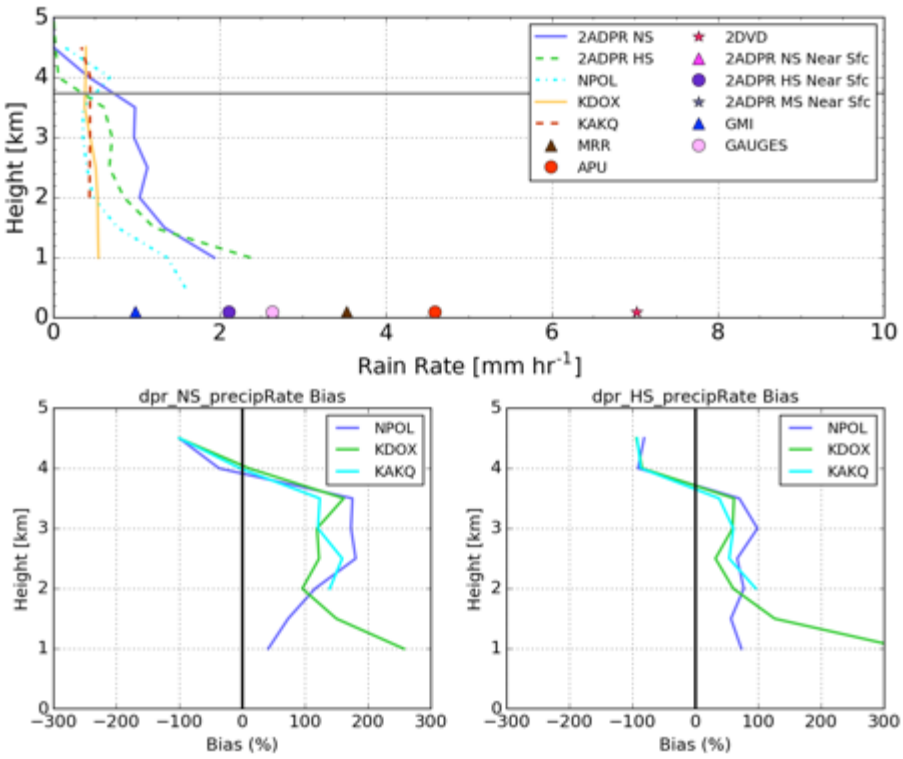

Figure 4: Mean rain rate (mm hr^{-1}) profiles from a number of platforms and algorithms (top) with bias plots for 2ADPR algorithm relative to ground radars (bottom). The horizontal solid line near 4.0 km indicates the freezing level.

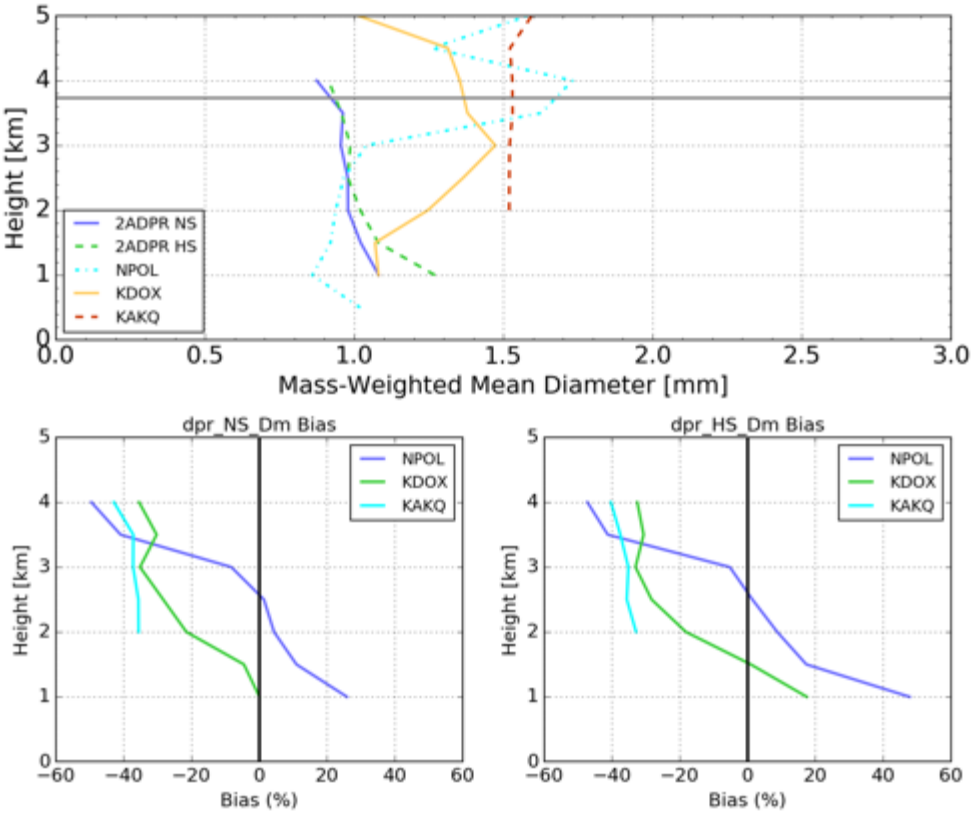

Figure 5: Mass weighted mean diameter, D_m (mm) profiles from various platforms (top) along with bias of 2ADPR algorithm relative to ground radars (bottom). The horizontal solid line near 4.0 km indicates the freezing level.

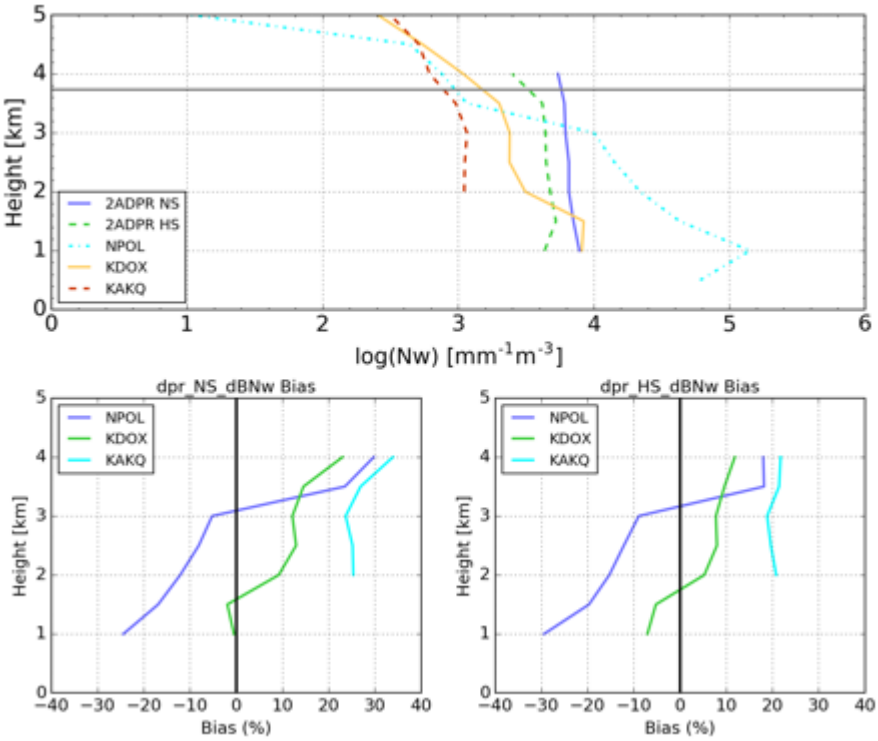

Figure 6: Mean normalized intercept parameter, Log N_w (mm^{-1} m^{-3}) profiles from various platforms (top) along with bias of 2ADPR algorithm relative to ground radars (bottom). The horizontal solid line near 4.0 km indicates the freezing level.

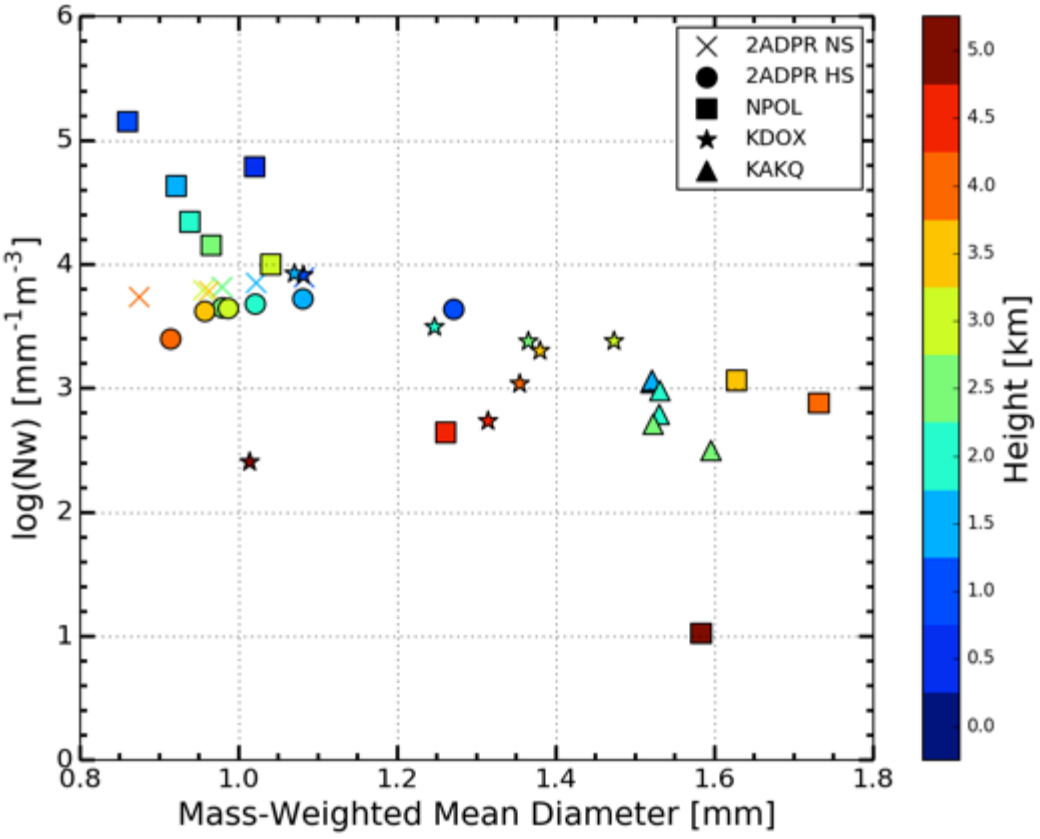

Figure 7: Mean Log N_w vs mean D_m symbols from the various instruments/algorithms for 21 May 2015 event as a function of height (colored). Cool colors are data near the surface while warm colors are from data above the surface regardless of instrument within the SIMBA grid column.

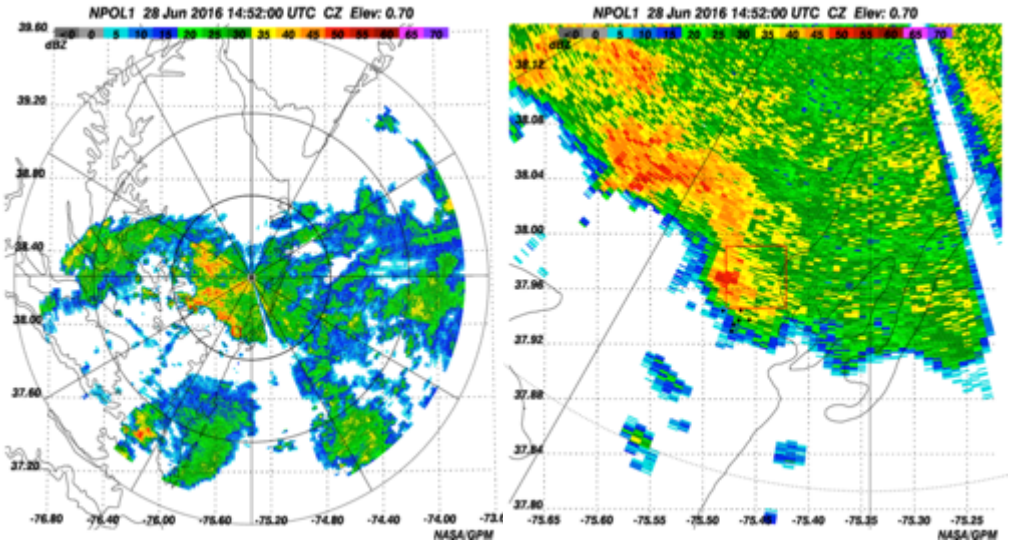

Figure 8: As in Figure 2 but for 28 June 2016, 145200 UTC at 0.7° elevation. Note the SIMBA grid box has been shifted to the north by 4.2 km from WFF Pad (see text for explanation) compared to the 21 May 2015 case.

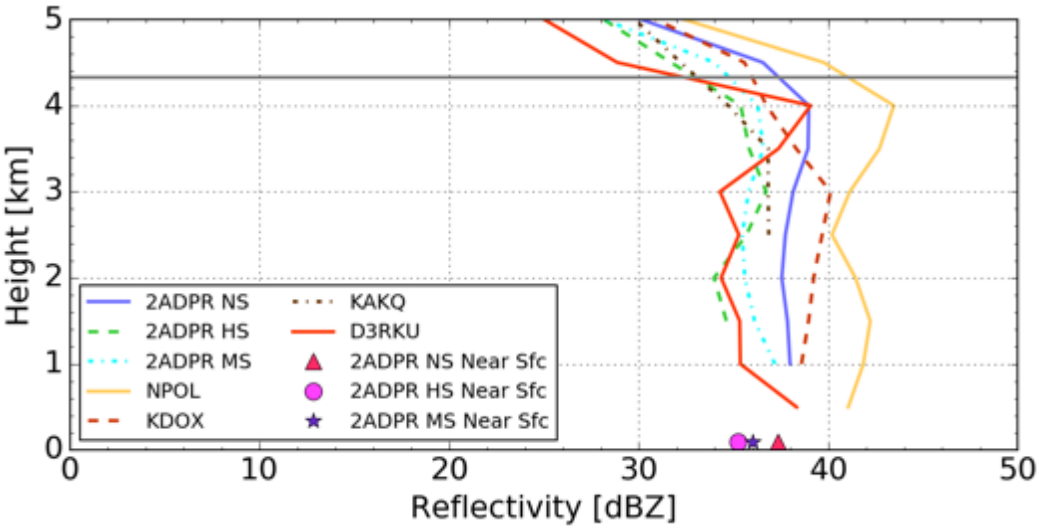

Figure 9: As in Figure 3 but for 28 June 2016 case. The horizontal solid line near 4.0 km indicates the freezing level.

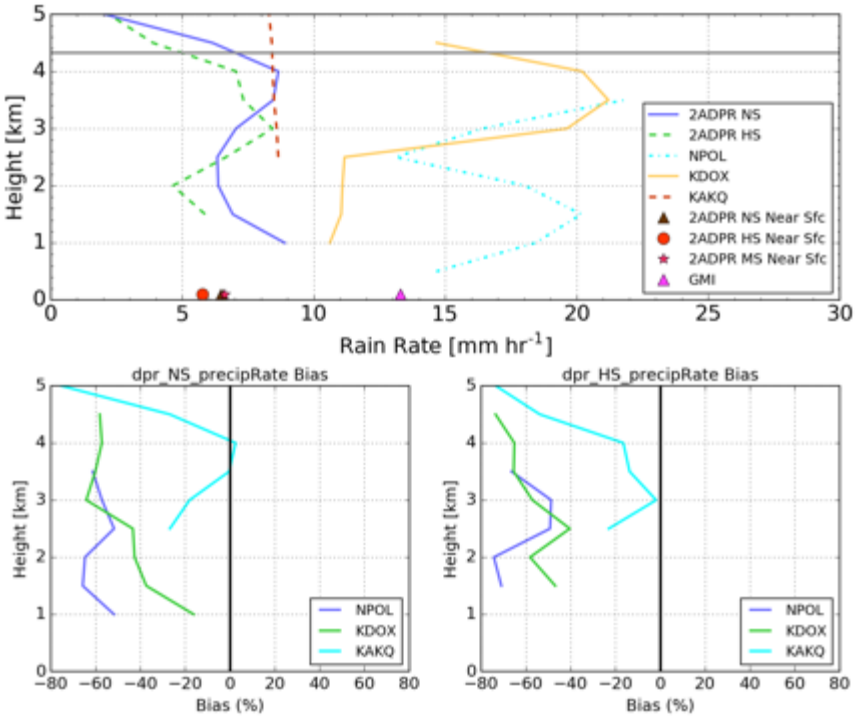

Figure 10: As in Figure 4 but for 28 June 2016 case. The horizontal solid line near 4.0 km indicates the freezing level.

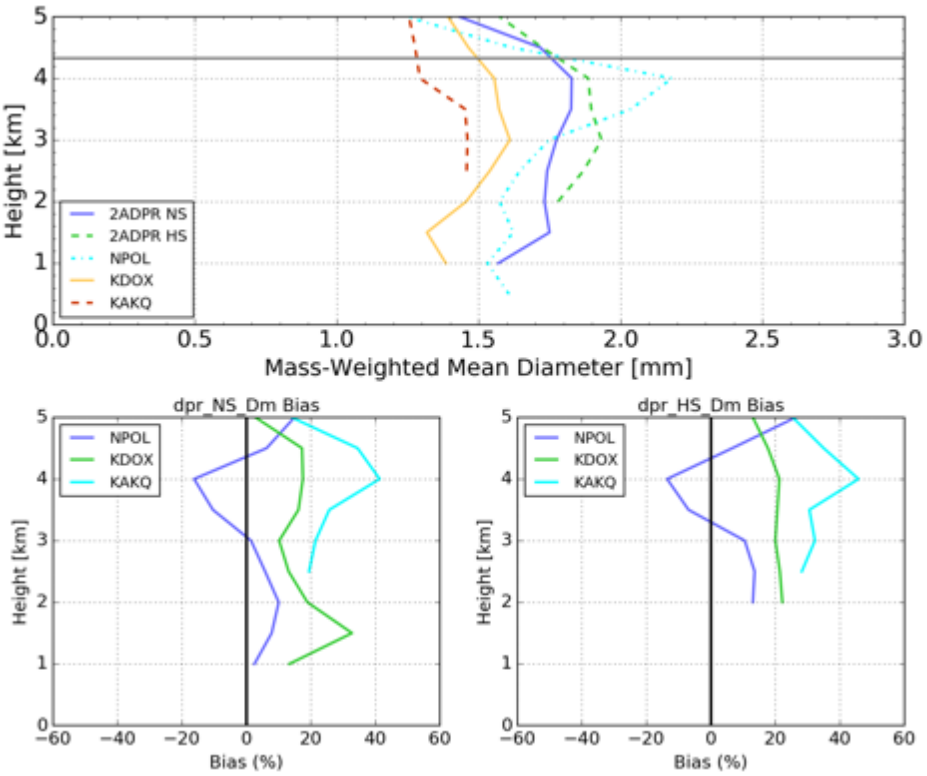

Figure 11: As in Figure 5 but for 28 June 2016 case. The horizontal solid line near 4.0 km indicates the freezing level.

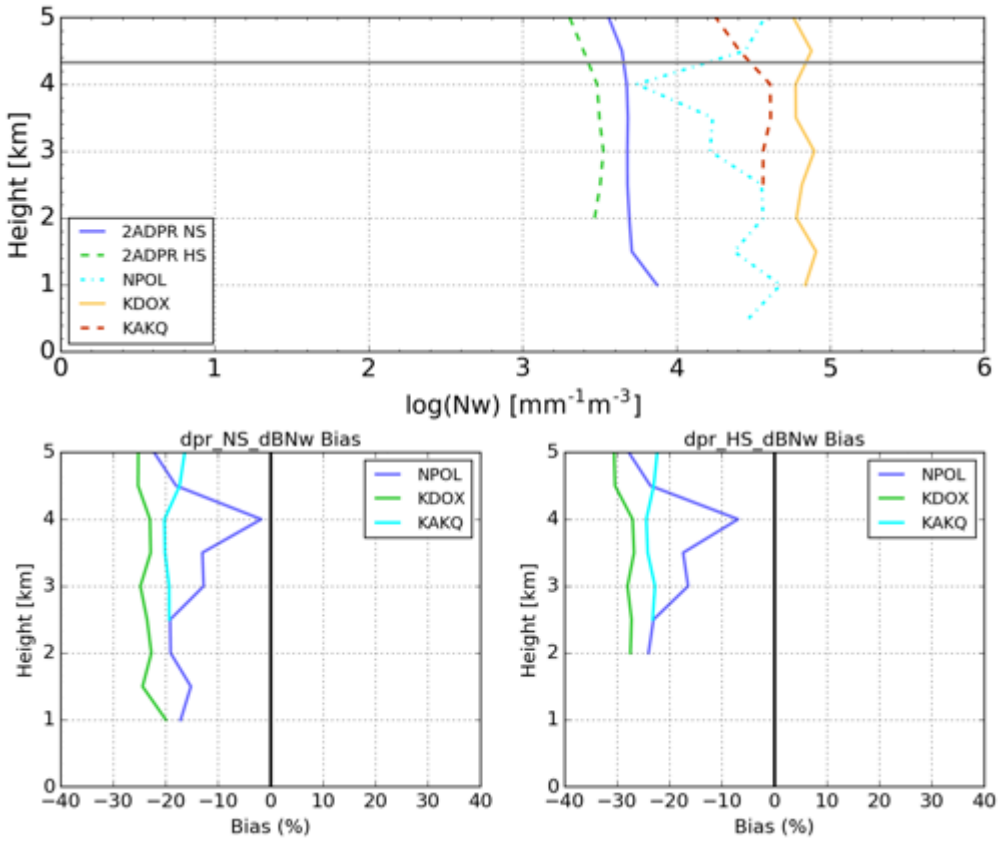

Figure 12: As in Figure 6 but for 28 June 2016 case. The horizontal solid line near 4.0 km indicates the freezing level.

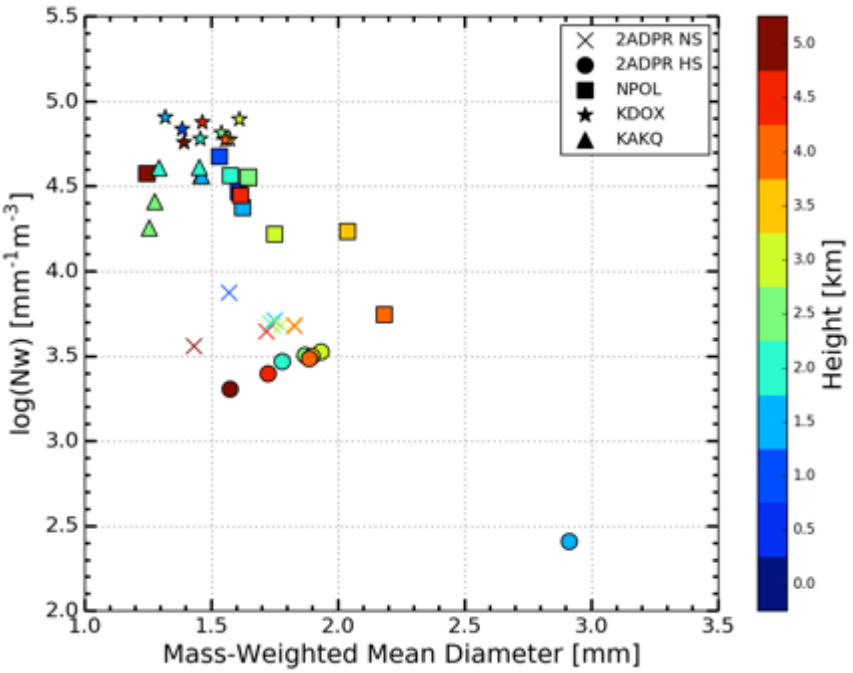

Figure 13: As in Figure 7 but for 28 June 2016 case.

21 May 2015	28 Jun 2016
NPOL RHI - 220420	NPOL RHI - 144947
KDOX PPI - 220400	KDOX PPI - 144934
KAKQ PPI - 220318	KAKQ PPI - 144631
D3R Ku RHI - 220154	D3R Ku RHI - 145054
APUs	N/A
2DVDs	N/A
Gauges	N/A
MRR	N/A
GMI GPROF V05	GMI GPROF V05
2ADPR V05	2ADPR V05

Table 1: Inventory list of data that went into SIMBA for data analysis for two different precipitation events. Note area of interest is the SIMBA column grid centered at the Wallops PRF (or WFF Pad) located at 37.93° Latitude and -75.47° Longitude. Distances from Wallops PRF for each ground-based instrument are listed: NPOL (38 km); KDOX (98 km); KAKQ (170 km); and D3R, MRR, APUs, 2DVDs, and Gauges all located at the Wallops PRF. Platform that was not available is listed as N/A. Ground scanning radar timestamps are included for reference.

2015_0521	MRR	APU	GAUGES	2DVD	GMI
GMI	-85.3	-78.5	-62.5	-85.9	X
2ADPR NS	-60.6	-42.6	0.23	-62.4	167.2
2ADPR HS	-68.5	-54.1	-19.9	-70.0	113.6
2ADPR MS	-60.6	-42.6	0.23	-62.4	167.2

2016-0628	GMI
GMI	X
2ADPR NS	-51.2
2ADPR HS	-56.7
2ADPR MS	-50.4

Table 2: GPM 2ADPR and GMI-GPROF bias error (%) of near surface rain rate algorithm for a) 21 May 2015 and b) 28 June 2016 rain events.